

2 **Km-scale polygonal sea-bed depressions in the Hatton Basin,**
3 **NE Atlantic Ocean - Constraints on the origin of polygonal**
4 **faulting**

5

6 Christian Berndt¹

7 *GEOMAR | Helmholtz Centre for Ocean Research, Kiel*

8

9 Colin Jacobs and Alan Evans

10 *National Oceanography Centre, Southampton, U.K.*

11

12 Aurélien Gay

13 *University of Montpellier 2, Montpellier, France*

14

15 Gavin Elliott

16 *Imperial College, London, U.K.*

17

18 David Long and Kenneth Hitchen

19 *British Geological Survey, Edinburgh, U.K.*

20

21

22 ¹Corresponding author: Christian Berndt, GEOMAR, Wischhofstr. 1-3, 24148 Kiel,
23 Germany, ph: +49 431 6002273; fax: +49 431 6002922; email: cberndt@geomar.de

24

25 **Abstract**

26 Polygonal faulting is a widespread phenomenon in sedimentary basins worldwide. It
27 changes basin-scale fluid flow patterns and alters the physical properties of the
28 sediments making it important for hydrocarbon exploration and geohazard analysis. It
29 is generally accepted that polygonal fault patterns derive from dewatering and
30 compaction of the host sediments, but there is debate regarding the processes that
31 control polygonal faulting. New multibeam-bathymetry data from the Hatton Basin,
32 NE Atlantic, show up to 10 m deep and 200-600 m wide troughs at the sea-bed. They

33 connect to each other forming polygons that are several hundred meters across, i.e. of
34 similar size as buried polygonal fault systems observed in 3D seismic data. The
35 troughs are symmetrical and resemble elongate pockmarks. Previously unpublished
36 high-resolution 2D seismic data from the same area show seismic disturbance zones
37 similar to pipes observed under pockmarks elsewhere as well as faults that have all
38 the characteristics of polygonal fault systems. The observation of the wide disturbance
39 zones is enigmatic, as they appear to follow the polygonal seafloor pattern. The
40 observed extent of the polygonal sediment contraction system is substantial covering
41 almost 37,000 km². We calculate that some 2600 km³ of possibly carbon-bearing
42 fluids have been expelled from this system and we expect that this will affect the
43 benthic ecosystems, although so far there is only limited evidence for chemosynthetic
44 habitats.

45

46 **Keywords:** Polygonal faulting; silicate diagenesis; dewatering; subsurface sediment
47 deformation; seismic data; multibeam bathymetry data

48 **1. Introduction**

49 Polygonal fault systems are networks of small-offset faults. They occur in layers of
50 fine-grained sediments within sedimentary basins. The faults occur in depth intervals
51 (tiers) that seem to be characterized by particularly small grain sizes. However, they
52 can extend for some distances into the over and underlying strata which makes them
53 important for the integrity of reservoirs that have polygonally faulted clays as cap
54 rock. Within the tiers polygonal faults strike in all directions but they tend not to
55 intersect at angles steeper than 10 degree which may be explained by the stress field
56 during propagation (Goult, 2008). For both reasons, i.e. layer confinement and
57 arbitrary strike direction, they cannot be caused by regional tectonic stresses
58 (Cartwright and Lonergan, 1996). Polygonal faults are up to several hundred meters
59 high and their throws are largest in the middle and decrease both top- and downward
60 (Berndt et al., 2003; Gay et al., 2004; Higgs and McClay, 1993; Stuevold et al., 2003).
61 Typically, the faults dip at angles of 30 to 70° against the vertical and the diameter of
62 the polygons is of the order of 1 to 2 km (Gay and Berndt, 2007) and their throw is
63 roughly increasing with fault plane height (Shin et al., 2010). Although polygonal
64 faults have been documented for more than 50 sedimentary offshore basins from
65 around the world onshore outcrop analogues are scarce (Cartwright et al., 2003).

66 Individual faults in the Ypern Clays, Belgium have been interpreted as the onshore
67 extension of the polygonal fault systems of the southern North Sea. They show
68 multiple mm-wide ruptures with limited displacement (Verschuren, 1992).

69

70 The non-tectonic origin of polygonal faults has been revealed by the use of 3D
71 seismic data in the 1990s (Cartwright, 1994). Apart from being little understood
72 structural phenomena, polygonal faults have some wide reaching implications that
73 merit further investigation. Work on the sedimentary basins off Norway (Berndt et al.,
74 2003) and Angola (Gay et al., 2004; Gay et al., 2003) demonstrated that the
75 polygonal faults are tightly linked to those basins' fluid flow systems. This is
76 evidenced by concentric sediment distortions that rise from the tip of the polygonal
77 faults and up to the sea-bed where they terminate in pockmarks. Although the faults
78 are believed to be linked to pore water expulsion and layer-parallel contraction of
79 sediments, it is not clear whether the fluids focused by the faults originate from
80 sediment dewatering from the deeper parts of the sedimentary basins or from the
81 polygonally faulted interval. The fact that polygonal faults are capable of focusing
82 fluid flow implies that their properties need to be understood for assessment of
83 reservoir leakage. As they only occur in fine-grained sediments they may also serve as
84 a good lithology indicator.

85

86 Five hypotheses for the origin of polygonal faults have been discussed in the literature
87 and were thoroughly reviewed in Cartwright et al. (2003), Cartwright (2011), and
88 Goult (2008). The first hypothesis is that the polygonal faulting is caused by
89 gravitational forces along gently dipping basins floors (Watterson et al., 2000). The
90 problem with this hypothesis is that polygonal faults have been observed in many
91 basins in which they are not bounded by a dipping surface at their base. Also the fact
92 that the faults strike in many different directions and have their greatest throw in the
93 middle of the faulted interval is not easily explained by this hypothesis. The second
94 hypothesis proposes the faulting to be initiated by Rayleigh Taylor instabilities due to
95 lighter under-consolidated sediments at the base of the polygonally faulted interval.
96 Indeed undulations of the expected wavelength are found at the top surface of a
97 polygonal fault tier in the Yper Clays (Henriet et al., 1991) and in the Faeroe Shetland
98 Trough (Davies et al., 1999) that extend to the surface (Long et al., 2004) and the total
99 horizontal shortening seems to be small in some polygonal fault systems (Watterson

100 et al., 2000). However, these are exceptions among the many observed polygonal fault
101 systems, and it is difficult to conceive how these density inversions should actually
102 lead to the observed faulting because it is very different from the structures in
103 response to salt related density inversions (Goult, 2008). The third hypothesis
104 invokes syneresis of colloidal sediments to initiate the initial fracturing of the rocks
105 (Cartwright and Dewhurst, 1998; Dewhurst et al., 1999). This process has been
106 observed in fine-grain sediments, but this hypothesis was questioned, as polygonal
107 faults occur in a wide range of lithologies and syneresis should be lithology
108 dependent. Laboratory experiments also indicate that this process is occurring very
109 fast (White, 1961) and it is difficult to see how it can lead to long-term deformation as
110 recorded by growth structures along polygonal faults. The fourth hypothesis invokes
111 faulting controlled by the residual shear strength of the faulted sediments (Goult,
112 2001; Goult, 2008; Goult and Swarbrick, 2005). This hypothesis was questioned
113 (Cartwright et al., 2003) because it requires initial weakness zones spaced at suitable
114 intervals and on its own would not explain the polygonal pattern. Furthermore this
115 hypothesis does not explain well how the faults propagate at larger scales (Cartwright,
116 2011). Instead Cartwright (2011) proposed that diagenetic processes in general are
117 responsible for a decreased ratio of horizontal to vertical stress which may facilitate
118 initial shear failure. This hypothesis is consistent with the vast extent of polygonal
119 fault systems and their organization in tiers. It is also consistent with laboratory
120 results for fine grained sediments (Shin et al., 2010).

121

122 The objective of this paper is to contribute to the understanding of the polygonal
123 faulting process by constraining the boundary conditions for the proposed hypotheses.
124 In particular we can provide further detail on the near surface structure of polygonal
125 faults and their overburden, the lithology in which such faults can occur, and the
126 relationship of polygonal faults and fluid expulsion structures. To this end we present
127 newly acquired multibeam bathymetry data and previously unpublished single
128 channel seismic data from the Hatton Basin, Northeast Atlantic (**Figure 1**).

129 **2. Data and Methods**

130 The data used in this study were acquired in the Hatton Basin and consist of
131 multibeam bathymetry data recorded with a SIMRAD EM120 system, which yields
132 15 m lateral and 1 m vertical resolution at about 1100 m water depth encountered in

133 the study area. We combined these data with the regional multibeam bathymetry
134 survey collected by the Geological Survey of Ireland. The single-channel seismic data
135 were acquired with the British Geological Survey (BGS) mini-airgun array which
136 consists of four 40 cubic inch guns with wave shape kits that operate at a pressure of
137 130 bar. The data were frequency filtered, deconvolved and post stack time-migrated
138 using water velocity. The vertical resolution is approximately 3 m at the sea-bed and
139 the shot interval is on average 15 m. These data were merged in a KingdomSuite
140 project with multi-channel seismic data from the southern Hatton Basin provided by
141 Irish Petroleum Infrastructure Programme (PIP). The still imagery and video footage
142 was recorded using a SEATRONICS DTS3000 deep water camera system, which
143 incorporates separate still and video cameras and a Valeport CTD. The data shown in
144 this paper were collected in a small area of the northern Hatton Basin (**Figure 1b**).
145 This area was chosen because it is surveyed with the BGS high-resolution seismic
146 system and ground-truthing by video observations is available.

147 **3. Observations**

148 **3.1. Bathymetry**

149 The multibeam bathymetric transects across the northern part of the Hatton Basin
150 show elongate depressions in the sea-bed that define approximately one hundred
151 polygons (**Figure 1b**). Thousands of polygons exist across the basin as a whole
152 covering an area of approximately 37,000 km² (Figure 1a). The depressions are up to
153 20 m deep, up to 400 m wide, and between 400 and 2000 m long (average 1500 m).
154 These depressions define the polygons which range from 500 to 5000 m in diameter.
155 A typical aspect ratio between the width of the sea-bed depressions and their length is
156 1:3. The slopes of the depressions are gentle and the overall shape is concave down.
157 The faults strike in all directions with a maximum to 080 (**Figure 1b**). The angles at
158 which the faults intersect are generally larger than 40 degree. The sea-bed inside the
159 polygons is flat and shows the same trend as the gentle regional topographic
160 variations. The polygons are only found in the central part of the Hatton Basin and
161 they gradually become less connected towards the east, south and west. Although
162 there is minimal multibeam bathymetry data in the north, the seismic data indicate
163 that here also the transition to un-deformed sea-bed at the margins of the basin is

164 gradual. The bathymetric data do not show evidence of sea-bed erosion in the centre
165 of the basin, but moats along the basin margins may be due to non-deposition/erosion.

166 **3.2. Seismic data**

167 The seismic data image the infill of the Hatton Basin. On top of the volcanic basement
168 (Laughton et al., 1972) there is a succession of up to 800 ms TWT-thick Eocene
169 sediments. Due to limited penetration of the BGS high-resolution data this unit is only
170 imaged in the PIP data in the southern part of the basin and at the rising flank of the
171 Rockall Bank in the BGS data in the north. Figure 2 shows a representative section of
172 the seismic line HA04-9005 from the southern part of the Hatton Basin. At depth it
173 shows the Eocene sediments draping onto the Rockall Bank and thicken towards the
174 centre of the basin. On top of this unit there is an up to 700 ms TWT-thick succession
175 of post Eocene to present sediments that is clearly influenced by bottom currents at its
176 southeastern end where it pinches out towards a moat against the Rockall Basin.

177 There are no signs of erosional unconformities within this unit, which is supported by
178 drilling at Site 982 (**Figure 3**).

179

180 There are a large number of vertical disturbances in the Oligocene to Recent
181 succession of the Hatton Basin (**Figure 4**). These disturbances can be divided into two
182 classes. Class 1 consists of zones of down-bending reflectors underneath the sea-bed
183 depressions. They extend from the sea-bed at 1700 ms TWT or 1200 m beneath sea
184 level down to the bottom of the recorded data at 2600 ms TWT in the north
185 corresponding to approximately 2000 m beneath sea level. Further south, the PIP data
186 show that these disturbance zones extend at least down to the top Eocene reflector.

187 Also the seismic facies of the Eocene succession just underneath the disturbance
188 zones is more chaotic than away from them, but it is not clear if this is real
189 deformation or the result of imperfect seismic imaging. The zones are between 200
190 and 400 m wide and their spacing is between 200 m and 2000 m. Generally seismic
191 amplitudes in these zones are reduced compared to the surrounding sedimentary
192 reflections. Some of these disturbances are asymmetrical with one side of the
193 disturbance being characterised by a gradual increase in reflector dip towards the
194 centre of the disturbance and a sharp offset of the reflectors on the other side. The
195 number of sharp offsets increases with depth. This is the result of some disturbance
196 zones being more focused at depth changing from gradually increasing dips to

197 discrete faults. Vertical spacing between seismic reflectors is greater in the hanging
198 walls indicating that these sediment disturbances are growth structures. Where the
199 boundaries of the sediment disturbance zones are sharp, i.e. fault like, the throw
200 increases with depth similar to polygonal fault systems elsewhere (Berndt et al., 2003;
201 Higgs and McClay, 1993; Stuevold et al., 2003).

202

203 The BGS high-resolution data lend themselves well for the study of the small-scale
204 nature of the sediment deformation structures. **Figure 4b** shows the detail of a class 1
205 disturbance with approximately 2 x vertical exaggeration, i.e. assuming 2 km/s P-
206 wave velocity. On a width of approximately 400 m within the depth interval from
207 1900 to 2500 ms TWT the reflections are interrupted. At the edges these disruptions
208 are frequently sharp and fault-like. Vertically they extend for up to 100 ms TWT. The
209 distance between offsets in the reflector packages is generally less than 80 m and
210 possibly less considering that the seismic line may cut them obliquely. We would like
211 to note, however, that the bathymetry (**Figure 1b**) shows, that seismic line BGS2000-
212 1-44 intersects the shown disturbance structure D at a steep angle and that this effect
213 would therefore be small. The horizontal extent of the disturbance structure coincides
214 with a vertical change of seismic facies that is continuous along the entire line. At its
215 base it coincides with the Top Eocene reflector (Reflector 4 of Laughton et al., 1972)
216 whereas at the top at approximately 1870 ms TWT it changes character where the
217 seismic amplitudes change from being higher above to being lower below. Above
218 1870 ms the wide disturbance zone is replaced by two normal faults that form a
219 graben above the disturbance zone.

220

221 The second class of seismic disturbance zones (class 2) is characterised by narrow 25-
222 75 m wide almost vertical zones of decreased seismic amplitudes. They are up to 500
223 ms TWT or 400 m high, i.e. 4-5 times higher than the faults observed in class 1
224 structures, and frequently occur in close vicinity to each other constituting groups of
225 two or three disturbances in the 2D seismic transects. These disturbance zones have
226 vertical displacements, i.e. throws, that increase with depth towards the centre of the
227 faults and decrease further down towards the lower tip of the faults similar to
228 polygonal faults elsewhere (Berndt et al., 2003; Cartwright and Dewhurst, 1998; Gay
229 et al., 2004; Lonergan et al., 1998). The dip of these faults ranges from 30 to 60
230 degrees against the vertical. However, as we only have 2D seismic available these are

231 apparent dips and may be steeper in instances where the faults are cut obliquely.
232 These disturbance zones are more abundant in the deeper part of the section of the
233 faulted interval. They do not reach the sea-bed anywhere on the seismic profiles
234 crossing these structures.

235

236 In summary it is the 200-400 m wide zones of chaotic seismic facies below 1870 ms
237 TWT and the much shorter vertical extent of faults in class 1 disturbances that
238 distinguishes this class from class 2. As the class 1 disturbances are often bounded by
239 sharp faults on either side in their top part, i.e. above 1870 ms TWT, this difference
240 cannot be the result of imaging one of the class 2 structures along strike.

241

242 Apart from the seismic disturbances of class 1 and the greater abundance of the
243 narrow seismic disturbances at depth the Oligocene to Pleistocene succession is
244 uniformly stratified. In particular, the seismic data do not show a polygonal fault
245 system underlying the wider (class 1) fluid expulsion structures, which is different
246 from offshore Angola and mid-Norway (Berndt et al., 2003; Gay et al., 2004).

247

248 The southeastern end of seismic profiles HA04-9005 (**Figure 2**) and BGS2000-1-1
249 (**Figure 5**) shows erosional truncation of the uppermost sedimentary reflections
250 against the sea-bed indicating submarine erosion. These top laps are limited to the
251 vicinity of the sea-bed moat that bounds the Hatton Basin to the east against Rockall
252 Bank. Submarine erosion was also reported for the western rim of the Hatton Basin
253 (Laughton et al., 1972), but this cannot be seen in our data. There is no seismic or
254 other evidence for erosion in the central parts of the basin.

255 *3.3. Video transect*

256 During a sea-bed survey in the summer of 2006 we collected a video transect across
257 one of the polygonal sea-bed depressions. There were no signs of fluid expulsion such
258 as vents or crusts of authigenic carbonates along this transect, and there were no
259 indications for abnormal sea-bed fauna such as pogonophora tube worms or cold
260 water coral reefs. The sea-bed shows, however, a large number of light patches which
261 may or may not be bacterial mats. This was corroborated by a recently conducted
262 ROV survey in 2011 (R. James, person. comm.).

263 4. Discussion

264 4.1. *Sea-bed polygons in the Hatton Basin and polygonal fault systems*

265 The polygonal sediment disturbance structures (**Figure 1**) developed in the post-
266 Eocene sediments of the Hatton Basin (Laughton et al., 1972). The depth of the basin
267 is not well known as basalts covered it during the Paleocene-Eocene and sediments
268 may underlie the volcanic succession. Wide angle seismic data indicate that it is at
269 least 2 and possibly 8 km deep (Morgan et al., 1989; Smith et al., 2005). In the study
270 area the post-volcanic sediments are approximately 1.5 km thick (Hitchen, 2004;
271 Laughton et al., 1972) and fill the trough between the Hatton Bank and the Rockall
272 Bank (**Figure 1**). The basin formed perhaps during the mid-Cretaceous (Smythe,
273 1989) as part of the rift history that led to continental break-up between the Rockall
274 Plateau and Greenland in the Early Eocene (Cole and Peachey, 1999).

275

276 The sediment deformation does not entirely consist of discrete faults, but shows a
277 continuum from laterally extensive inflexions of the seismic reflectors at shallow
278 depth to discrete faults deeper in the sediment pile. The vertical extent of the faults is
279 quite variable. While some extend from the top-Eocene reflector almost to the surface
280 others appear as part of a network of fractures (**Figure 4b**). In other respects, i.e. the
281 length of the polygon sides, the variation in strike directions, and variation in throw,
282 they are similar to other polygonal fault systems (**Figure 2**, (Gay and Berndt, 2007;
283 Lonergan et al., 1998). The fact that they almost reach the surface and are overlain by
284 tip folds that ultimately form the sea-bed depressions makes the system in the Hatton
285 Basin similar to the polygonal fault systems on the Gjallar Ridge (Clausen et al.,
286 1999) and offshore Angola (Cartwright and Dewhurst, 1998; Gay et al., 2004).

287

288 The faults occur in Oligocene to recent sediments that were sampled at DSDP Site
289 116 and 117 (Laughton et al., 1972) and ODP Site 982 (Shipboard Scientific Party,
290 1996). At Site 116 and 982 the sediments consist of approximately 700 m of
291 biogeneously oozes with very high calcareous carbonate content (~80%). Only the
292 glacially influenced upper 70 m of sediments have significant amounts of detritus.
293 Beneath 70 m the sediments are increasingly more lithified from watery oozes at the
294 top to limestones at 700 m depth. Also the silica is transforming to chert from
295 approximately 550 m depth. However, the density is only reaching 2.05 g/cm³ at the

296 bottom of Site 116, i.e. at 854 m depth below the seafloor, and seismic velocities
297 measured with the core logger do not exceed 1.7 km/s even at the base of the
298 borehole, both indicating that dewatering due to silica diagenesis was active but not as
299 pronounced as elsewhere in the North Atlantic (Berndt et al., 2004; Davies et al.,
300 2008) where silica diagenesis leads to the development of bottom simulating
301 reflectors which is not observed in the Hatton Basin. The post Eocene sedimentary
302 succession was deposited without a recognised hiatus and with sedimentation rates of
303 fairly constant 3 cm / 1000 years coinciding with increasing paleo-water depths. The
304 paleontological data indicate neritic sedimentation for the Early Eocene at Site 117
305 and after a late Eocene hiatus a gradual increase of water depth until the present water
306 depth of approximately 1200 m. Overall, the continuous pelagic sedimentation in the
307 Hatton Basin has caused particularly high water contents which may be the reason
308 why the polygonal fluid escape patterns are so well developed.

309

310 The type of available seismic data, i.e. limited bandwidth and short streamer length,
311 does not lend itself to an extensive analysis of pore fill. However, there are some
312 observations that suggest that the class 1 deformations are evidence for past or present
313 fluid migration. First and foremost, it is the disturbance of the primary seismic
314 reflections which is typically observed underneath seep sites (Berndt et al., 2003;
315 Hovland and Judd, 1988). Secondly, there is a general decrease of amplitude within
316 the chaotic zones, which may be the result of pore water expulsion from more water
317 rich layers and a resulting decrease in acoustic impedance contrasts. We interpret the
318 sediment disturbance structures in the Hatton Basin as a polygonal fault system
319 although the occurrence of numerous fluid escape structures of class 1 makes it
320 somewhat unusual. While the polygonal arrangement of seafloor depressions may be
321 explained by the polygonal faults at depth and their accompanying tip folds, it is more
322 difficult to explain a polygonal arrangement of the class 1 deformation structures at
323 depth. In the 2D seismic data they appear as groups of fractures (**Figure 4b**). But it is
324 not clear how they should develop into polygons if they do not propagate as faults due
325 to the stress focusing at their lateral tips (Goult, 2008). They are not underlain by a
326 mature polygonal fault system (Figure 2), which may lead to a polygonal shape of
327 fluid escape.

328

329 An explanation may be found in the observations related to the class 2 anomalies.
330 These are in fact only solitary, i.e. not elongate or joined-up, features such as pipes
331 underlying pockmarks elsewhere. As we do not have 3D seismic control in this area
332 we cannot be sure that they link up in polygons. In this case they may be the result of
333 hydro-fracturing during dewatering of the basin. They may therefore serve as zones of
334 weakness from which polygonal faults nucleate due to their reduced residual strength
335 of the sediments (Goult, 2008). The fact that the seismic amplitudes decrease lateral
336 consistently at about 1900 ms TWT could be explained by a diagenetic change of
337 silica from opal A to opal CT (Berndt et al., 2004) and it is tempting to attribute the
338 change of style in class 1 disturbance zones to the increased dewatering connected to
339 this diagenetic transformation. However, the changes of silica concentration and type
340 observed at Site 116 do not show abrupt variations (Laughton et al., 1972), and the
341 seismic data do not show a clear crosscutting of this amplitude anomaly across the
342 primary sedimentary reflections, which may of course be explained by the horizontal
343 stratification. Thus, the silica control cannot be corroborated with the available data.
344 We also do not find clear evidence for a transition from class 1 to class 2 which would
345 be expected at the nucleation points, but this may well be due to the limited amount of
346 seismic data. It would take high-resolution 3D seismic data to observe a class 1
347 structure starting at a class 2 structure.

348 ***4.2 Timing – The Hatton Basin a site of present-day polygonal faulting***

349 The polygonal structures of the Hatton Basin reach almost up to the sea-bed and
350 neither the DSDP/ODP drilling results nor the seismic data show evidence for erosion
351 at the present sea-bed. This means that the polygonal pattern develops at shallow
352 burial depth, although proper faulting is not observed until some 30-50 m beneath the
353 sea-bed. In this sense the polygonal sediment disturbances are similar to the structures
354 observed on the Gjallar Ridge on the Norwegian Margin (Clausen et al., 1999) and
355 offshore Angola (Cartwright and Dewhurst, 1998; Gay et al., 2004; Gay et al., 2003).
356 Polygonal deformation affects the sediments above C30 of Hitchen (2004). This
357 means polygonal faulting in the Hatton Basin could be a continuously ongoing
358 process since the Miocene. This is similar to the Norwegian Margin for which the
359 distribution of dewatering pipes that are related to polygonal faulting indicate
360 protracted activity of the polygonal fault system over several million years (Berndt et
361 al., 2003; Gay and Berndt, 2007).

362

363 The absence of discrete faults in the upper strata coincides with the change in
364 lithology, i.e. the increase in detritus in the uppermost 70 m caused by the glacial
365 influence. It is not clear if this change in character of the polygonal deformation is a
366 sign for shut-down of the polygonal faulting caused by the change in lithology or
367 whether the focusing of the polygonal deformation would propagate into the present
368 sea-bed sediments with continued burial. The latter seems more likely as the upper
369 termination of the faults is variable and not confined to this depth only.

370 *4.3 Nucleation – polygonal fault changes with depth*

371 The observations from the Hatton Margin provide further constraints on the formation
372 of polygonal sediment dewatering. The sediment densities encountered at DSDP Site
373 116 show that there is no inversion at present which rules out Rayleigh-Taylor
374 instabilities in recent times (Davies et al., 1999; Victor and Moretti, 2006), i.e. the
375 first hypothesis discussed by Cartwright et al. (2003). However, if past density
376 inversion was related to undercompaction it may have disappeared during pressure
377 release and fluid expulsion, and it may be difficult to find evidence for it now.
378 Furthermore, the polygonal fault pattern is symmetrical (**Figure 1**), and the seismic
379 data show that the polygonal sediment deformation occurs in a confined basin
380 without a regionally dipping base. This makes gravitational forces (Watterson et al.,
381 2000) an unlikely agent for the development of the polygonal pattern, at least in this
382 area.

383

384 Of the four hypotheses proposed by Cartwright et al. (2003) this leaves syneresis and
385 fracturing as a result of low residual shear strength (Goult, 2001; Goult and
386 Swarbrick, 2005). Furthermore, diagenetic processes may reduce the ratio of
387 horizontal to vertical effective stress (k_0) necessary to initiate shear failure
388 (Cartwright, 2011; Shin et al., 2008). The new data show that the dewatering fluids
389 disturb the sediments in a polygonal pattern and it is likely that the disruption caused
390 by pore water movement decreases the shear strength of the sediments. It is therefore
391 of fundamental importance to understand whether polygonal faults develop first (and
392 focussing of fluid flow by the polygonal faults results in the fluid escape structures
393 above), or if fluid expulsion comes first and is already organised in a polygonal
394 geometry when the polygonal faults develop. This may be supported by the

395 observations that (1) the fluid escape seems to be organised in polygons without
396 polygonal faults underneath each of the fluid escape features, (2) the fluid escape
397 features are considerably bigger than the polygonal faults, and (3) most of the
398 polygonal faults do not reach the sea-bed and the sediment deformation is more
399 confined downward, which perhaps indicates that it takes time for the polygonal faults
400 to develop, and that weakness zones are forming as a result of fluid flow focusing.

401

402 Dewatering may provide weakness zones that are required by the residual shear
403 strength hypothesis. On the other hand, dewatering will at least partly be related to
404 diagenetic changes. The results of Shin et al., (2010) show that this in itself may
405 generate initial shear failures that develop into polygonal faults. As such the proposed
406 residual shear strength and diagenetic weakening hypotheses are partly
407 complementary as faulting may start at dewatering structures and propagate laterally
408 and upward due to reduced k_0 that is caused by diagenetic processes.

409

410 With the limited data at hand it seems most likely that the fluid expulsion structures
411 develop first, followed by polygonal faulting within these weakness zones. The
412 sediment contraction caused by dewatering finally induces further faults within the
413 polygons. These faults only develop at depths at which protracted sediment
414 contraction has generated the necessary reduction of horizontal stress. Overall this
415 process seems to be rather slow and continuous instead of vigorous and episodic,
416 because there are no reflectors in the seismic data that bend upwards toward the fluid
417 pathways which may be expected for fast sediment deforming eruptions. This is
418 supported by the absence of distinct fluid seeps in the video data or pockmarks in the
419 multibeam bathymetry data.

420

421 Our observations lend support to an important role of diagenesis in sediment
422 deformation. The observed variations in silica composition at Site 116 show a general
423 decrease in opal A concentration down-hole. Applied to the experimental results of
424 Shin et al., (2010) this would mean that the entire basin is subject to decreased k_0
425 facilitating initial shear failure. Possibly in some places, i.e. the class 1 deformations,
426 the fluid expulsion from diagenetic processes is so vigorous that focused fluid flow
427 systems form.

428 ***4.4 Dewatering of the Hatton Basin and implications for seabed ecology***

429 The new data clearly show that the small offset faults and associated sea-bed
430 depressions are not an analogue to the Feni Drift sediments as proposed previously
431 (Laughton et al., 1972). The sea-bed polygons observed in the multibeam bathymetry
432 data clearly disprove the previous interpretation of the sea-bed depressions seen in 2D
433 seismic data as NE-SW trending sea-bed furrows caused by bottom currents.

434

435 The seismic and multibeam data indicate that the sea-bed polygons occur over some
436 37,000 km² in the central part of the Hatton Basin. Using an average thickness of 700
437 m of sediments that are affected by the polygonal deformation and a porosity loss
438 from 80 to 60 % (based on results from DSDP Hole 116) within this interval
439 (Laughton et al., 1972), we calculate that approximately 2600 km³ of fluids could
440 have been expelled from this system. If the structures reported by Vanneste et al.
441 (1995) are part of the same sediment body these numbers may still be significantly
442 bigger. So far, it is unknown if this volume is expelled continuously or episodically,
443 but the fact that the deformation zones reach the sea-bed to form polygons shows that
444 the fluid expulsion has been active until the recent geological time, i.e. during
445 deposition of the present surface sediments.

446

447 During a sea-bed survey in the summer of 2006 we collected a video transect across
448 one of the polygonal sea-bed depressions. This did not reveal conclusive evidence for
449 active fluid expulsion such as vents or indicative chemosynthetic benthic ecosystems
450 such as tube worms. The video images do show a large number of pale patches at the
451 sea-bed which may be bacterial mats, and decimetre-scale relief which is uncommon
452 in distal, deep-water areas such as the Hatton Basin (**Figure 6**). This relief may
453 indicate crusts of authigenic carbonates along the video transect. This may indicate
454 episodic expulsion of fluids as continuous dewatering would yield negligible fluxes
455 and would unlikely result in clearly observable carbonate crusts. It is possible that
456 future investigation of this vast area will result in the discovery of benthic ecosystems
457 that have adapted to this special habitat. In addition to the shelter that is provided by
458 the hummocky sea-bed, it is possible that the polygonal dewatering structures sustain
459 chemosynthetic ecosystems such as those recently found in the vicinity of other cold
460 seep sites (Sibuet and Olu-Le Roy, 2003).

461 ***4.4. Implications from other types of patterned ground***

462 Joint-bounded polygonal columns develop in a wide variety of materials ranging from
463 millimetres to hundreds of meters in diameter. Contraction of cooling, solidified
464 magma yields columns that are much taller than broad. This process is called
465 columnar jointing and occurs in almost any kind of solidified lava (DeGraff and
466 Aydin, 1987). Polygonal patterns called desiccation cracks also form when mud
467 (Weinberger, 2001) or starch (Müller, 1998) dry out. In these cases the columns are
468 usually as wide as they are high. Furthermore, polygonally patterned ground develops
469 in permafrost environments, where it is related to complex cycles of freezing, melting
470 and development of secondary ice lenses (Lachenbruch, 1962; Marchant et al., 2002).
471 The new data extend this list of polygonal surface patterns to submarine surface
472 sediment dewatering. The polygons found in the Hatton Basin constitute an end-
473 member in terms of polygon size. The only reported somewhat similar systems are the
474 sediment structures in Lake Superior (Cartwright et al., 2004). However, these
475 structures are not polygonal-shaped but doughnut-shaped and they are not linked to
476 polygonal faults at depth.

477

478 The polygonal sediment deformation in the Hatton Basin and polygonal fault system
479 in general are characterised by a higher density of faults at depth than at the surface.
480 This is opposite to polygonal joints that develop in basalts (Saliba and Jagla, 2003) or
481 starch (Goehring and Morris, 2005). Saliba and Jagla (2003) calculate how the stress
482 pattern varies with depth, and that joining of the discontinuity leads to a focusing of
483 displacement with depth and duration of cooling. There are two fundamental
484 differences between columnar jointing and the polygonal sediment deformation in the
485 Hatton Basin. Whereas desiccation cracks and columnar jointing are governed by
486 dispersive laws and starts at the surface and migrates down, polygonal faults nucleate
487 at depth and migrate up and their genesis is probably linked to convective laws of
488 fluid migration. Columnar jointing in basalts also starts at once when lava solidifies,
489 whereas the polygonal sediment deformation in the Hatton Basin develops during
490 ongoing sedimentation and for several millions of years. The fact that the fault density
491 in the Hatton Basin is greater at depth than it is at the surface may therefore imply that
492 the structures at the surface are more mature in the sense that the stress due to
493 contraction and water expulsion has focused. It would require high-resolution 3D

494 seismic data to determine the geometry of the fault terminations at depth and to
495 quantify the stress regime. This geometry information is necessary for finite element
496 modelling of the stress field.

497

498 Müller (1998) conducted a quantitative comparison between the column diameter in
499 columnar joints in starch and basalt and concluded that in a first approximation the
500 column diameter depends on the depth gradient of the polygon forming physical
501 property, i.e. the temperature gradient for cooling basalt and the water content for
502 drying starch. Columnar jointing in basalt has a much greater diameter and the
503 temperature gradient is roughly three orders of magnitude lower than the starch
504 gradients agreeing qualitatively with a two orders of magnitude greater diameter for
505 the basalt columns. Following this argument the large diameter of the polygon size of
506 the dewatering structures in the Hatton Basin would suggest even lower gradients in
507 water content. This is intuitively the case in a slowly compacting sedimentary basin in
508 which the water content decreases from 62-68 % volume in the surface sediments to
509 55 % volume at 700 m depth (Laughton et al., 1972). However, the water content is
510 very variable. Even at 700 m depth there are still sections in which the water content
511 is in excess of 80% indicating the importance of focused fluid migration for these
512 sediments.

513 **5. Conclusions**

514 Polygonal fault development is closely linked to the alignment of fluid escape features
515 in a polygonal pattern. The large-scale pattern seems to be governed by a stress-
516 induced alignment of fluid escape pathways. These in turn may provide the weakness
517 zones required for residual shear strength controlled initial failure. It is crucial that 3D
518 seismic data are collected in the Hatton Basin to corroborate the polygonal layout of
519 the fluid escape pathways, which so far is only deduced from the alignment of the
520 polygonal seafloor patterns with the class 1 disturbance zones in the 2D seismic data.
521 We also suggest that geotechnical experiments be conducted on samples from DSDP
522 Site 116 or the close-by ODP Site 982 to see if their lithology is conducive to
523 syneresis or if there is a correlation between the amount of diagenetically induced
524 horizontal contraction and the depth intervals at which polygonal faulting is best
525 developed.

526

527 The hypothesis that the gradient of the property that governs stress build-up, i.e. the
528 reduction in water content, controls the size of the polygons may be valid over very
529 different scales. The polygonal faults in the Hatton Basin extend the scale that was
530 established for millimetre to decimetre-sized polygon patterns to the kilometre size. In
531 this sense, even the development of polygonal faults in a marine environment can be
532 considered as drying of a surface layer. Although of course, the faulting nucleates and
533 propagates at depth and up to the surface. Continuum mechanics have successfully
534 been applied to the modelling of the polygonal patterns within columnar jointed
535 basalts (Saliba and Jagla, 2003). Similar models should be applied to the polygonal
536 fault system in the Hatton Basin in order to predict the length of time that it takes to
537 develop the polygonal patterns, but this would require three-dimensional imaging of
538 the polygonal system at depth.

539 **6. Acknowledgements**

540 The bathymetric data and imagery from the northern part of the Hatton Basin was
541 funded as part of the UK Department of Trade and Industry's offshore energy
542 Strategic Environmental Assessment (SEA) programme, and collected aboard the SV
543 Kommandor Jack. This work was partly funded through the EC Hermes project
544 GOCE-CT-2005-511234-1. We thank the Geological Survey of Ireland for permission
545 to publish the multibeam bathymetry data from the south of the Hatton Basin, and the
546 British Geological Survey and the Petroleum Infrastructure Programme for permission
547 to use their seismic data. DL and KH publish with permission of Executive Director
548 British Geological Survey (NERC).

549 **7. References**

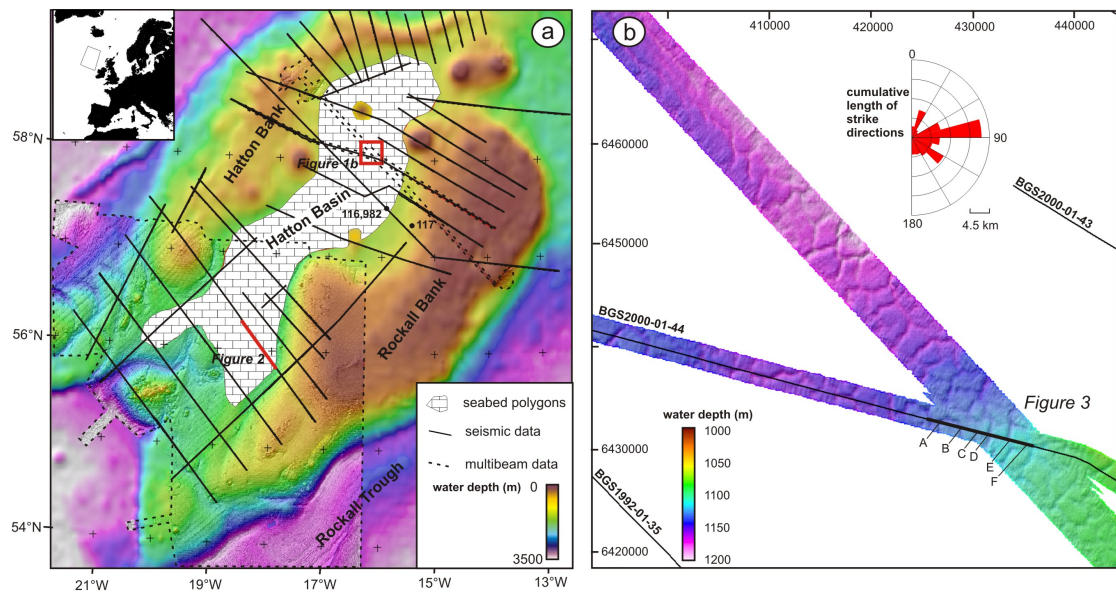
- 550 Berndt, C., Bünz, S., Clayton, T., Mienert, J. and Saunders, M., 2004. Seismic
551 character of bottom simulating reflectors: examples from the mid-Norwegian
552 margin. *Marine and Petroleum Geology*, 21: 723-733.
- 553 Berndt, C., Bünz, S. and Mienert, J., 2003. Polygonal fault systems on the mid-
554 Norwegian margin: A long term source for fluid flow. In: P. van Rensbergen,
555 R.R. Hillis, A.J. Maltman and C.K. Morley (Editors), *Subsurface Sediment*
556 *Mobilization*. Special Publication. Geological Society of London, pp. 283-290.
- 557 Cartwright, J.A., 1994. Episodic basin-wide hydrofracturing of overpressured Early
558 Cenozoic mudrock sequences in the North Sea Basin. *Marine and Petroleum*
559 *Geology*, 11(5): 587-607.
- 560 Cartwright, J.A., 2011. Diagenetically induced shear failure of fine-grained sediments
561 and the development of polygonal fault systems. *Marine and Petroleum*
562 *Geology*, 28(9): 1593-1610.

- 563 Cartwright, J.A. and Dewhurst, D.N., 1998. Layer-bound compaction faults in fine-
564 grained sediments. *Bulletin of the Geological Society of America*, 110(10):
565 1242-1257.
- 566 Cartwright, J.A., James, D. and Bolton, A., 2003. The genesis of polygonal fault
567 systems: a review. In: P. van Rensbergen, R.R. Hillis, A. Maltman and C.K.
568 Morley (Editors), *Subsurface Sediment Mobilization*. Geological Society of
569 London, pp. 223-243.
- 570 Cartwright, J.A. and Lonergan, L., 1996. Volumetric contraction during the
571 compaction of mudrocks: a mechanism for the development of regional-scale
572 polygonal fault systems. *Basin Research*, 8: 183-193.
- 573 Cartwright, J.A., Wattrus, N., Rausch, D. and Bolton, A., 2004. Recognition of an
574 early Holocene polygonal fault system in Lake Superior: Implications for the
575 compaction of fine-grained sediments. *Geology*, 32(3): 253-256.
- 576 Clausen, J.A., Gabrielsen, R.H., Reksnes, P.A. and Nysether, E., 1999. Development
577 of intraformational faults in the northern North Sea: influence of remote
578 stresses and doming of Fennoscandia. *Journal of Structural Geology*, 21:
579 1457-1475.
- 580 Cole, J.E. and Peachey, J., 1999. Evidence for pre-Cretaceous rifting in the Rockall
581 Trough: an analysis using quantitative plate tectonic modelling. In: A.J. Fleet
582 and S.A. Boldy (Editors), *Petroleum Geology of Northwest Europe*:
583 *Proceedings of the 5th conference*. Geological Society of London, pp. 359-
584 370.
- 585 Davies, R., Cartwright, J.A. and Rana, J., 1999. Giant hummocks in deep-water
586 marine sediments: Evidence for large-scale differential compaction and
587 density inversion during early burial. *Geology*, 27(10): 907-910.
- 588 Davies, R.J., Gouly, N.R. and Meadows, D., 2008. Fluid flow due to advance of
589 basin-scale silica reaction fronts. *Bulletin of the Seismological Society of*
590 *America*, 120: 195-206.
- 591 DeGraff, J.M. and Aydin, A., 1987. Surface morphology of columnar joints and its
592 significance to mechanics and direction of joint growth. *Geological Society of*
593 *America Bulletin*, 99: 605-617.
- 594 Dewhurst, D.N., Cartwright, J.A. and Lonergan, L., 1999. The development of
595 polygonal fault systems by syneresis of colloidal sediments. *Marine and*
596 *Petroleum Geology*, 16: 793-810.
- 597 Gay, A. and Berndt, C., 2007. Cessation/reactivation of polygonal faulting and effects
598 on fluid flow in the Vøring Basin, Norwegian Margin. *Journal of the*
599 *Geological Society*, 164: 129-141.
- 600 Gay, A., Lopez, M., Cochonat, P. and Sermondadaz, G., 2004. Polygonal faults-
601 furrows system related to early stages of compaction - upper Miocene to
602 recent sediments of the Lower Congo Basin. *Basin Research*, 16: 101-116.
- 603 Gay, A. et al., 2003. Sinuous pockmark belt as indicator of a shallow buried turbiditic
604 channel on the lower slope of the Congo basin, West African margin. In: P.
605 van Rensbergen, R.R. Hillis, A. Maltman and C.K. Morley (Editors),
606 *Subsurface Sediment Mobilization*. Special Publication. Geological Society of
607 London, pp. 173-189.
- 608 Goehring, L. and Morris, S.W., 2005. Order and disorder in columnar joints.
609 *Europhysics Letters*, 69(5): 739-745.
- 610 Gouly, N.R., 2001. Polygonal fault networks in fine-grained sediments - an
611 alternative to the syneresis mechanism. *First Break*, 19: 69-73.

- 612 Goult, N.R., 2008. Geomechanics of polygonal fault systems: a review. *Petroleum*
613 *Geoscience*, 14: 389-397.
- 614 Goult, N.R. and Swarbrick, R.E., 2005. Development of polygonal fault systems: a
615 test of hypotheses. *Journal of the Geological Society*, 162: 587-590.
- 616 Henriot, J.-P., de Batist, M. and Verschuren, M., 1991. Early fracturing of Paleogene
617 clays, southernmost North Sea: relevance to mechanisms of primary
618 hydrocarbon migration. In: A.M. Spencer (Editor), *Generation, Accumulation*
619 *and Production of Europe's Hydrocarbons*. European Association of Petroleum
620 Geologists Special Publication. Oxford University Press, Oxford, U.K., pp.
621 217-227.
- 622 Higgs, W.G. and McClay, K.R., 1993. Analogue sandbox modelling of Miocene
623 extensional faulting in the Outer Moray Firth. In: G.D. Williams and A. Dobb
624 (Editors), *Tectonics and Sequence Stratigraphy*. Geological Society, London,
625 pp. 141-162.
- 626 Hitchen, K., 2004. The geology of the UK Hatton-Rockall margin. *Marine and*
627 *Petroleum Geology*, 21(8): 993-1012.
- 628 Hovland, M. and Judd, A.G., 1988. Seabed pockmarks and seepages. Impact on
629 biology, geology and the environment. Graham and Trotman, London.
- 630 Lachenbruch, A.H., 1962. Mechanics of thermal contraction cracks and ice-wedge
631 polygons in permafrost. *Geological Society of America Bulletin*, 70: 1-69.
- 632 Laughton, A.S., Berggren, W.A. and al., e., 1972. Initial reports of the Deep Sea
633 Drilling Project, Volume XII, Washington (U.S. Government Printing Office)
- 634 Lonergan, L., Cartwright, J.A. and Jolly, R.J.H., 1998. The geometry of polygonal
635 fault systems in Tertiary mudrocks of the North Sea. *Journal of Structural*
636 *Geology*, 20: 529-548.
- 637 Long, D., Bulat, J. and Stoker, M.S., 2004. Sea bed morphology of the Faroe-Shetland
638 Channel derived from 3D seismic datasets. In: R.J. Davies, J.A. Cartwright,
639 S.A. Stewart, M. Lappin and J.R. Underhill (Editors), *3D seismic Technology:*
640 *application to the exploration of sedimentary basins*. Memoir. Geological
641 Society, London, pp. 53-61.
- 642 Marchant, D.R. et al., 2002. Formation of patterned ground and sublimation till over
643 Miocene glacier ice in Beacon Valley, southern Victoria Land, Antarctica.
644 *Geological Society of America Bulletin*, 114(6): 718-730.
- 645 Morgan, J.V., Barton, P.J. and White, R.S., 1989. The Hatton Bank continental
646 margin - III. Structure from wide-angle OBS and multichannel seismic
647 refraction profiles. *Geophysical Journal International*, 98: 367-384.
- 648 Müller, G., 1998. Starch columns: Analog model for basalt columns. *Journal of*
649 *Geophysical Research*, 103(B7): 15,239-15,253.
- 650 Saliba, R. and Jagla, E.A., 2003. Analysis of columnar joint patterns from three-
651 dimensional stress modeling. *Journal of Geophysical Research*, 108(B10):
652 doi:10.1029/2003JB002513.
- 653 Shin, H., Santamaria, C. and Cartwright, J.A., 2010. Displacement field in
654 contraction-driven faults. *Journal of Geophysical Research*, 115(B07408):
655 doi:10.1029/2009JB006572.
- 656 Shin, H., Santamarina, J.C. and Cartwright, J.A., 2008. Contraction-driven shear
657 failure in compacting uncemented sediments. *Geology*, 36(12): 931-934.
- 658 Shipboard Scientific Party, 1996. Site 982. In: E. Jansen, M.E. Raymo, P. Blum and
659 and others (Editors), *Proceedings of the Ocean Drilling Project, Initial*
660 *Reports*. Ocean Drilling Program, College Station, TX, pp. 91-138.

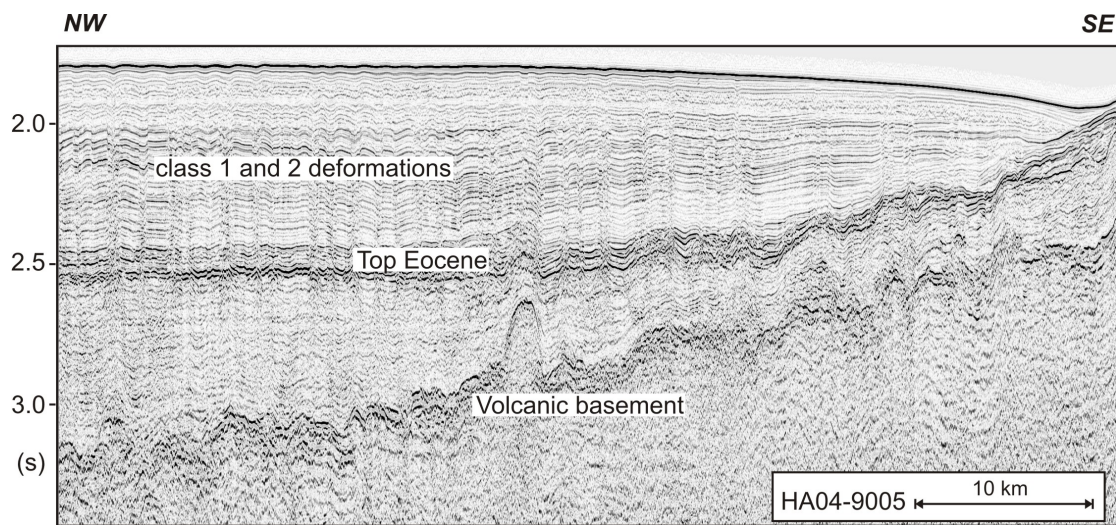
- 661 Sibuet, M. and Olu-Le Roy, K., 2003. Cold seep communities on continental margins:
662 structure and quantitative distribution relative to geological and fluid venting
663 patterns. In: G. Wefer et al. (Editors), *Ocean Margin Systems*. Springer
664 Verlag, Berlin, pp. 235-251.
- 665 Smith, L.K., White, R.S., Kuszniir, N.J. and Team, i., 2005. Structure of the Hatton
666 Basin and adjacent continental margin. In: A.G. Doré and B.A. Vining
667 (Editors), *Petroleum Geology: North-West Europe and Global Perspectives -*
668 *Proceedings of the 6th Petroleum Geology Conference*. Geological Society,
669 London, pp. 947-956.
- 670 Smythe, D.K., 1989. Rockall Trough - Cretaceous or Late Paleozoic? *Scottish Journal*
671 *of Geology*, 25: 5-43.
- 672 Stuevold, L., Faereth, R.B., Arnsen, L., Cartwright, J. and Möller, N., 2003.
673 Polygonal faults in the Ormen Lange Field, Møre Basin, offshore mid-
674 Norway. In: P. Van Rensbergen, R.R. Hillis, A. Maltman and C.K. Morley
675 (Editors), *Subsurface Sediment Deformation*. Geological Society, London, pp.
676 263-282.
- 677 Vanneste, K., Henriët, J.-P., Posewang, J. and Theilen, F., 1995. Seismic stratigraphy
678 of the Bill Bailey and Lousy Bank area: implications for subsidence history.
679 *Geological Society, London, Special Publications*, 90(1): 125-139.
- 680 Verschuren, M., 1992. An integrated approach to clay tectonic deformation, and
681 development of a new 3D surface modeling method, University of Ghent, 359
682 pp.
- 683 Victor, P. and Moretti, I., 2006. Polygonal fault systems and channel boudinage: 3D
684 analysis of multidirectional extension in analogue sandbox experiments.
685 *Marine and Petroleum Geology*, 23(7): 777-789.
- 686 Watterson, J., Walsh, J., Nicol, A., Nell, P.A.R. and Bretan, P.G., 2000. Geometry and
687 origin of a polygonal fault system. *Journal of the Geological Society*, 157:
688 151-162.
- 689 Weinberger, R., 2001. Evolution of polygonal patterns in stratified mud during
690 desiccation: The role of flaw distribution and layer boundaries. *Geological*
691 *Society of America Bulletin*, 113(1): 20-31.
- 692 White, W.A., 1961. Collodial phenomena in sedimentation of argillaceous rocks.
693 *Journal of Sedimentary Petrology*, 31: 560-570.
694
695

696 **Figures**

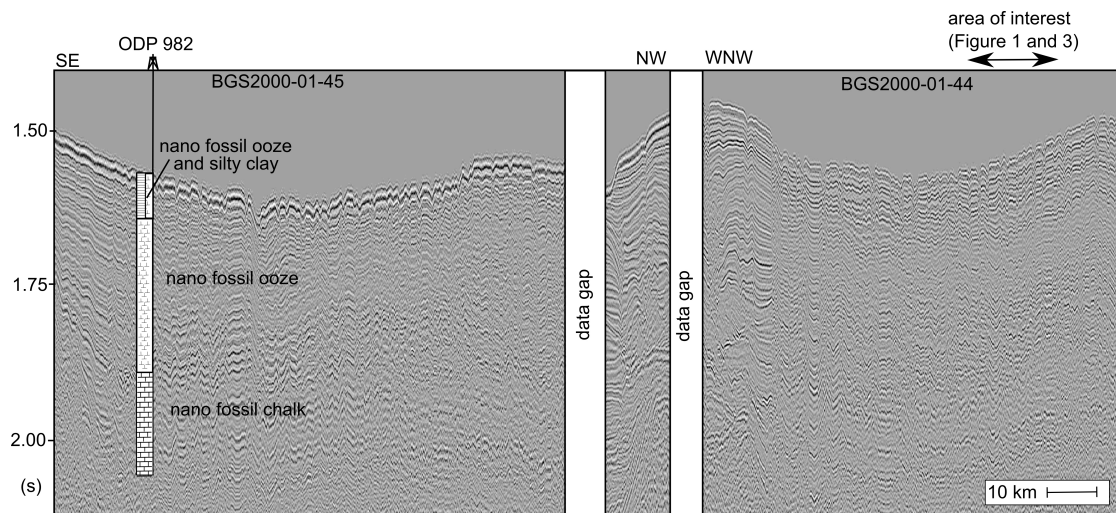


697
 698 Figure 1: The polygonal sediment deformation structures are observed in the northern
 699 part of the Hatton Basin. 1b) Multibeam bathymetry data showing polygonal sea-bed
 700 depressions and the strike directions of the sea-bed depressions.

701



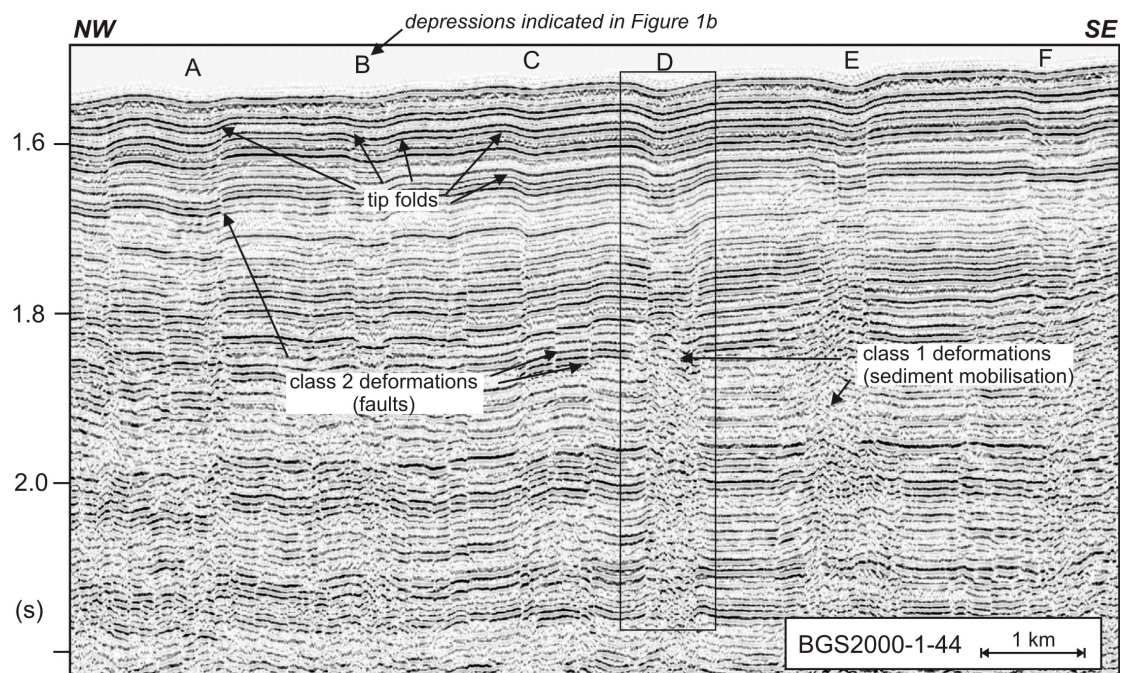
702
 703 Figure 2: Regional profile (see Fig. 1 for location) showing the depth at which the
 704 polygonal deformations terminate at the Top Eocene reflector (reflector 4 of Laughton
 705 et al., 1972).



706

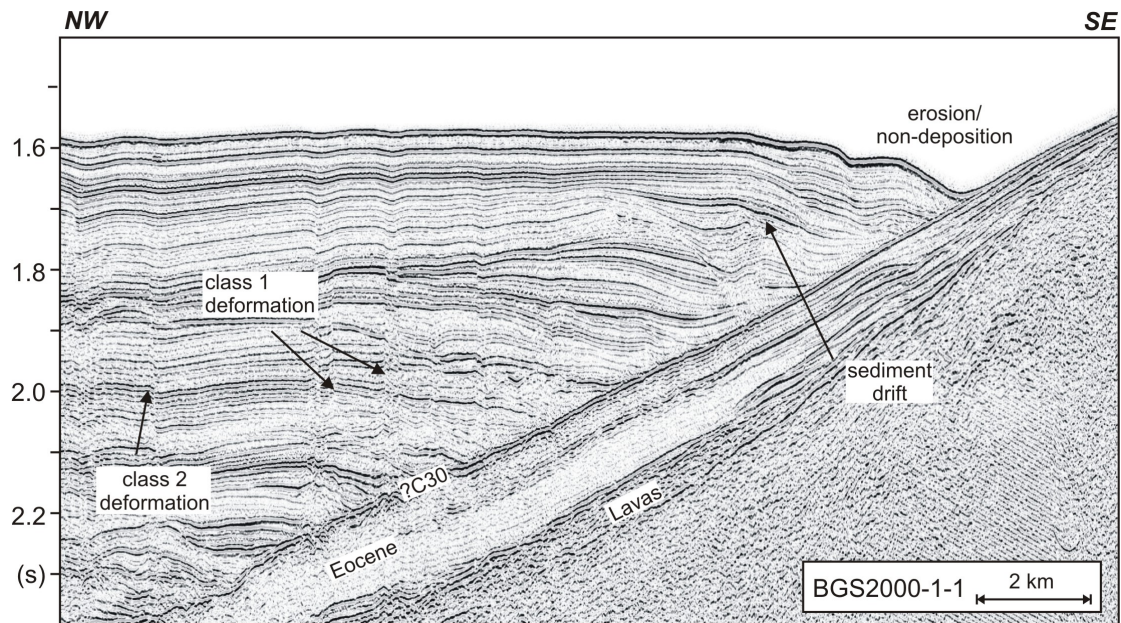
707 Figure 3: Correlation of the ODP Site 982 lithology to the area with multi-beam
 708 bathymetry coverage further north (Figure 1 for location). For the depth conversion of
 709 the borehole depth we used seismic velocities of 1600 m/s and 2000 m/s for the top
 710 and lower part of the hole.

711



712

713 Figure 4: Single-channel seismic line intersecting the multibeam bathymetry transect.
 714 The arrows B and C at the top indicate the location of sea-bed depression annotated in
 715 Figure 1b. Note, different types of sediment deformation and vertical variation in
 716 deformation style. 3b) Seismic example with approximately 2 x vertical exaggeration
 717 showing the nature of the class 1 deformations and the typical 30-50 degree dip of the
 718 polygonal faults.



719

720 Figure 5: Single-channel seismic line from the northeastern parts of the Hatton Basin.

721 The Late Eocene and younger sediments overlie the volcanic successions of the

722 Rockall High. The sea-bed is scoured by bottom currents leading to erosion or non-

723 deposition at the flank of the Rockall High. C30 as defined by Hitchen (2004).

724



725

726 Figure 6: Video still showing the small-scale topography and pale patches within one

727 of the polygonal sea-bed depressions. These may result as bacterial mats from fluid

728 escape. For scale: the fish is approximately 20 cm long.